TUB41: A Robust MOF for Industrial Gas Separation

Robert Oestreich,[1#] Marcus N. A. Fetzer,[1#] Andreas Schreiber,[3] Alexander Knebel,[4,5] Markus Suta,[2] Christoph Janiak [1]* and Gündoğ Yücesan[1]*

1. Institute for Inorganic Chemistry and Structural Chemistry, Heinrich-Heine-University Düsseldorf, Universitätsstr. 1, D-40225 Düsseldorf, Germany.
2. Inorganic Photoactive Materials, Institute for Inorganic Chemistry and Structural Chemistry, Heinrich Heine University Düsseldorf, Universitätsstr. 1, 40225 Düsseldorf, (Germany
3. Microtrac Retsch GmbH, Retsch-Allee 1-5, 42781 Haan
4. Otto Schott Institute of Materials Research, Center for Energy and Environmental Chemistry II, Friedrich Schiller University Jena, Lessingstraße 12-14, D-07743 Jena, Germany.
5. Center for Energy and Environmental Chemistry, Friedrich Schiller University Jena, Philosophenweg 7a, D-07743 Jena, Germany

# These authors contributed equally to this work.

E-mail: guendog.yuecesan@hhu.de and janiak@hhu.de

Keywords: Chemically & Thermally Stable MOFs, CO_2 Capture, Gas Separation

Herein, we report on the thermal and chemical stability and CO_2 and water vapor adsorption of a mixed linker phosphonate-MOF [Cu(4,4'-bpy)$_{0.5}$(1,4-NDPAH$_2$)], namely TUB41 (bpy = bipyridine and NDPAH$_4$ = naphthalenediphosphonic acid). TUB41 exhibits reversible phase transitions upon heating until 330 °C. TUB41 is a very stable MOF across a pH range of 1 to 11 and after two years of repeated adsorption experiments and activation at 80 °C and ambient humidity. While gases with larger kinetic diameter do not access the narrow pores of TUB41, it can efficiently adsorb CO_2 and water vapor, which have smaller kinetic diameter compared to other atmospheric gases. TUB41 exhibits a moderate enthalpy of adsorption for CO_2, which is favorable compared to water vapor at low pressure, indicating its potential for selective CO_2 separation in the presence of water vapor. TUB41 has an estimated optical band gap between 2.7 and 3.0 eV, which is within the bluish-violet range.

1. Introduction

Metal organic frameworks (MOFs) have evolved as one of the most studied material classes with a wide range of potential industrial applications in medicine, food chemistry, catalysis, energy storage, and many others. [1-4] For each application, MOFs must possess unique chemical and thermal stability suitable for the desired application. For example, biodegradability is an essential requirement for MOFs to be used for applications such as drug delivery,[5-9] while MOFs intended for use in batteries, supercapacitors, electrocatalysis (including hydrogen evolution and oxygen evolution reactions, or HER and OER, respectively), CO_2 capture, and water harvesting must demonstrate sufficient stability to survive in the presence of electrolytes, water, and acidic or basic environments.[10] Despite, the rich structural diversity of MOFs and their vast potential applications,[2] there still is only a handful of MOFs in the literature, which are considered to be stable in the presence of water, acids, bases and electrolytes.[11,12] Notably, UiO-66, which is known for its exceptional stability, has a shelf lifetime of ca. 2 months at room temperature and ambient humidity.[13,14] Therefore, the development of next-generation stable MOFs will be the most significant breakthrough that will finally open the gateway towards the industrial application of MOFs. The secondary building units (SBUs) of conventional carboxylate MOFs are usually composed of water-labile metal carboxylate clusters, including Zr(IV) carboxylate clusters (as in UiO-66), which limit conventional MOF applications in aqueous medium.[14] Furthermore, a CO_2 adsorption process also generates an acidic environment, which is challenging for conventional MOFs to survive for a long period of time.[15] Therefore, we have recently focused on the development of chemically stable unconventional organic linkers, that can generate high affinity metal binding to create water insoluble SBUs, that are resistant to hydrolysis in aqueous environment. For example, phosphonic acids are very robust organic linkers surviving in the presence of concentrated acids, and the P-C bond is known to be stable in the presence of UV-light and high temperature.[16,17] Furthermore, phosphonates are known to produce non-soluble salts with transition metal ions.[16,18,19]

Metal phosphonates have been emerging as a versatile MOF family, demonstrating exceptional chemical stability across a wide range of conditions.[20-22] Our group and others have reported the stability of early phosphonate-MOFs in harsh environments, including strong acids, bases, and even aqua regia, making them highly promising candidates for diverse applications such as electrocatalysis, energy storage, and sequestration of greenhouse gases.[16,21,23,24] Additionally, our investigations into hydrogen-bonded organic frameworks (HOFs) and polyphosphonate

covalent organic frameworks (COFs) constructed from phosphonic acids have shown exceptional stability in humid environments during and after proton conductivity experiments.[25-28] It has been also shown that metal phosphonates might be electrically conductive.[4,29,30] Despite these developments in the field, there are only a few phosphonate-MOFs that have been reported in the literature, and the further development of phosphonate-MOFs remains constrained by the limited commercial availability of arylphosphonic acid linkers and fundamental phosphonate precursors.[20] Addressing these challenges is significant to establish novel sustainable MOF families that are stable in the presence of harsh chemical environment for applications such as batteries, CO_2 capture, electrocatalysis, etc.

In this work, we wanted to focus on naphthalene as a linker core, which is a fundamental hydrophobic and polyaromatic moiety to create MOFs that might capture hydrophobic gases.[31] Previously, we published a structural report on TUB41, which was a mixed-linker MOF utilizing 1,4-naphthalenediphosphonic acid (1,4-NDPAH_4) and 4,4'-bipyridine (4,4'-bpy) (See Figure 1a).[32] Due to its very low yield, we were not able to work on its applications previously. TUB41 has narrow hydrophobic pores, which are suitable for sequestering molecules with small kinetic diameters such as CO_2 and H_2O. In this work, we were able to synthesize TUB41 hydrothermally as a single product phase and we explored its chemical and thermal stability. We furthermore used it to capture CO_2, and explored its optical properties.[32] We have also shown that TUB41 has a shelf lifetime of beyond 2 years after repeated gas adsorption and activation at 80 °C under vacuum, which is a strong improvement compared to the conventional carboxylate-based MOFs such as UiO-66 (2 months).

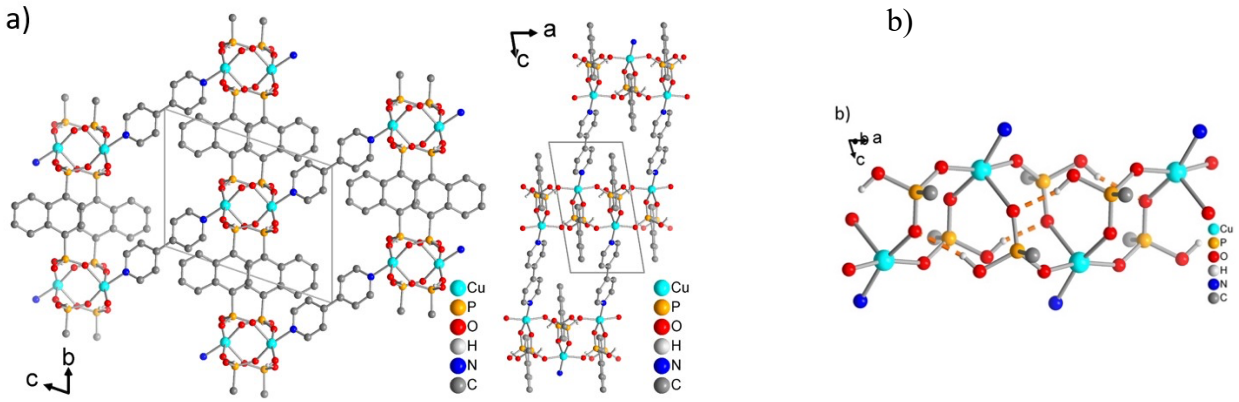

Figure 1. a) Section of the packing in the crystal structure of phosphonate-MOF TUB41 along two different viewing directions (hydrogen atoms on carbon are omitted for clarity). b) Infinite secondary building unit of TUB41 running along the *a* direction, also showing the hydrogen bonds between the phosphonate groups.

In more detail, as shown in Figure 1b, TUB41 has a rod-shaped SBU composed of typical eight membered Cu-O-P-O-Cu-O-P-O rings observed in phosphonate MOFs, which are bridged by the square pyramidal Cu(II) atoms, while the hydrogen bonding between the Cu(II) coordinating phosphonate groups defines the final shape of the SBU and provides an hydrophilic character to the SBU. On the other hand, hydrophilic hydrogen bonded SBUs of TUB41 are surrounded by hydrophobic naphthalene moieties hypothetically limiting the non-covalent interactions of the SBU with hydrophilic gases, and generating a more suitable environment for hydrophobic gases such as CO_2. Recently, MOF research has focused on frameworks with narrow pore sizes to enhance gas adsorption selectivity.[33] The combination of narrow pore sizes and the hydrophobic nature observed in TUB41, along with its thermal and chemical stability, makes it highly desirable for the development of industrial applications of MOF that can selectively capture or separate hydrophobic gases such as CO_2. [34,35]

2. Chemical Stability of TUB41

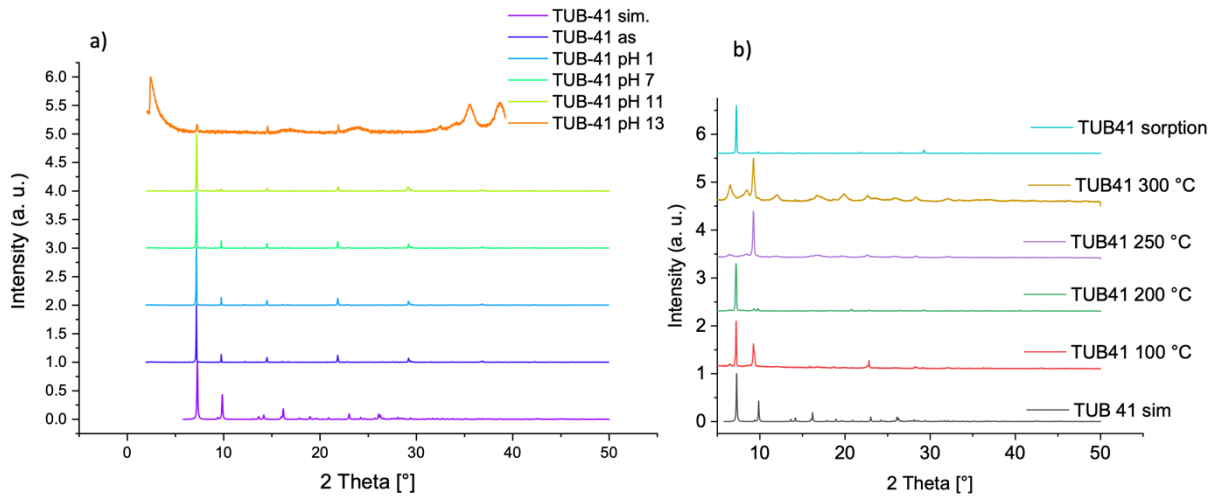

Figure 2. a) PXRD (Cu K_α radiation) of TUB41 at different pH, and b) at different temperatures and after adsorption experiments.

The crystals of TUB41 were reproduced in Fall 2022. Chemical stability tests of TUB41 were performed by suspending TUB41 crystals in aqueous solutions with different pH in HCl between 1 and 13 for 2 hours. In addition, TUB41 samples were left in the hydrothermal reaction mixture for 1 month before the purification of the crystals that indicates its stability in aqueous medium of pH 2.5 for ca. one month. As depicted in Figure 2a, the powder X-ray diffraction (PXRD) data of the acid- and base-treated samples of TUB41 retains its PXRD pattern between pH1 and pH 11 after 2 hours, suggesting its stability in acidic environment for

this period of time and basic environment at pH 11. The MOF sample treated at pH 13 starts to decompose, although the sample retains some of the original PXRD pattern. It has been predominantly converted into CuOH species, indicating relatively slow decomposition at pH 13. In addition, TUB41 was synthesized in Parr acid digestion reaction vessels in distilled water at pH 1.5 (pH 2.5 after the reaction) and 120 °C for 48 hours, which also suggests the intrinsic chemical stability of TUB41 in acidic environment.

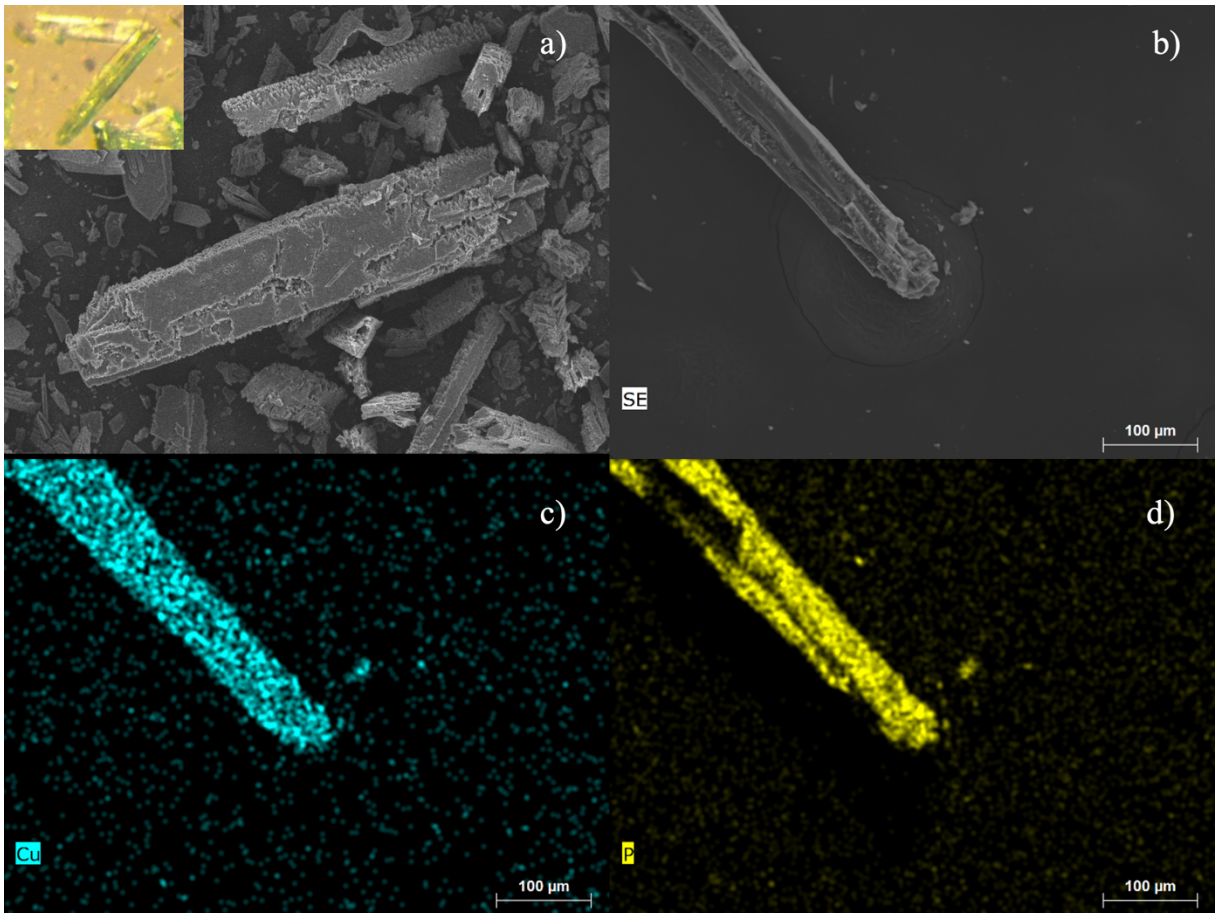

Figure 3. SEM pictures of TUB41 after adsorption experiments. a) and b) the crystals of TUB41, and the corresponding element mapping c) Cu d) P.

As can be seen in Figure 3, SEM pictures indicate that the crystals mostly retain their morphology after two years of repeated adsorption experiments and storage at room temperature and ambient humidity.

3. Thermal Stability of TUB41

In order to understand the thermal behavior of TUB41, we initially performed powder X-ray diffraction (PXRD) of samples which were heated up to 300 °C for one-hour periods, and

collected the PXRD data after cooling them to room temperature (Figure. 2b). Phosphonic acids condense at high temperatures to make P–O–P bonds and this also suggested by MS-TGA as water evaporation is gradually observed above ca. 250 °C, TUB41 potentially leading to crystalline metal polymeric framework at ca. 300 °C (See Figure 2 and MS-TGA section).[28] TUB41 has a rod shaped SBU composed of corner-sharing continuous eight-membered Cu–O–P–O–Cu–O–P–O rings (see Figure 1b).

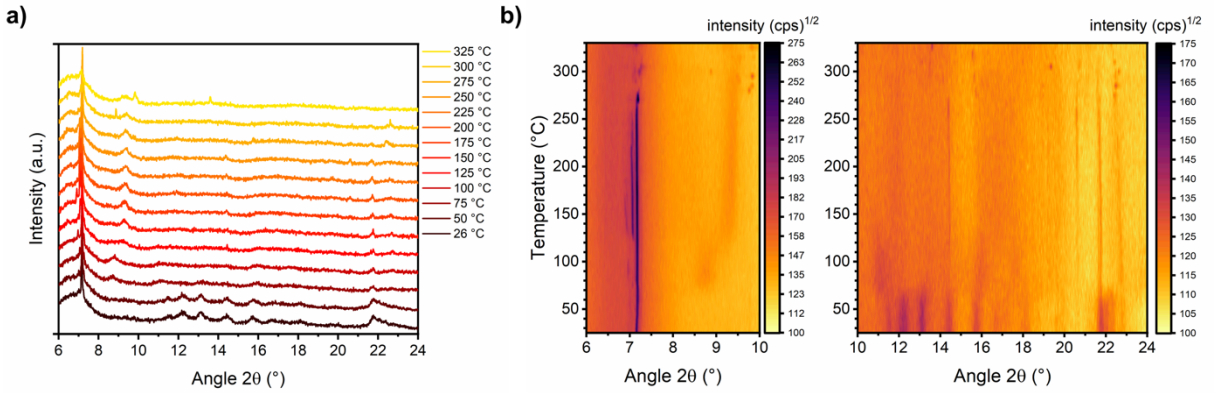

Figure 4. a) In-situ VT-PXRD (Cu K_α radiation) in a staggered plot until 330 °C, showing no drastic changes of the PXRDs over a long 2θ range. b) Contour plots of TUB41 from 25-330 °C using the square-root scaling of the intensity, allowing us to follow changes in crystallinity and phase transformations better. Dark areas correlate 2θ values to observed high intensity of reflections.

To gather insights on the stability of the material after several years of cycling, we measured in-situ variable temperature powder x-ray diffraction (VT-PXRD) using the two-year-old crystals, which were repeatedly used in CO_2 and water vapor adsorption measurements up to 330 °C. As it can be seen in Figure 4a, PXRD pattern remained very similar to the original phase until 330 °C, while some minor phase transformations can be observed. The phase transformation and the thermal stability of the compound is better observed in contour plots of TUB41 in Figure 4b, with the dark areas showing crystalline, consistent Bragg reflections with varying intensity continuing until 330 °C. At $2\theta = 7.2°$ the most interesting reflex is observable, which splits into two peaks above 120 °C and reverts above 250 °C, demonstrates the strongest phase transformation, which dis- and re-appears above 280-330 °C infrequently. Between 14° and 25° many smaller, but observable transformations occur. At $2\theta = 14.4$, 20.5, 21.8 and 22.4° reflections are sharpening from temperatures above 80°C on, demonstrating higher crystallinity of the sample until 330 °C (see Figure 4b). We previously summarized the conformational

changes in flexible rod shaped SBUs observed in phosphonate MOFs.[36] The observed phase transitions might be a result of the reversible conformational changes in the Cu–O–P–O–Cu–O–P–O rings. As depicted in Figure 1b, the rod-shaped SBU of TUB41 has repeating hydrogen bonds between the mono-deprotonated phosphonate-based hydrogen atom and Cu(II)-coordinated phosphonate oxygen atoms. The thermal flexibility of the TUB41 might be originating from the breaking and reforming of the hydrogen bonds leading to multiple SBU conformations and phase transitions at different temperatures.

4. MS coupled thermogravimetric analysis.

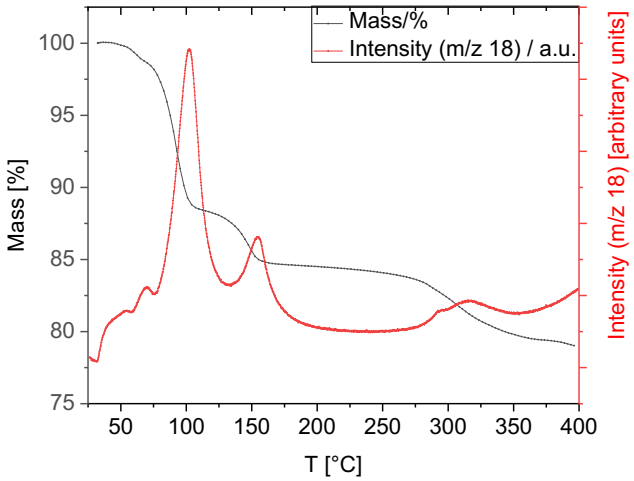

Figure 5. TGA-MS measurements in synthetic air for TUB41.

We have performed MS-coupled thermogravimetric analysis (TGA) to understand the thermal behavior of TUB41 (SI for instrumental details). As depicted in Figure 4, MS-TGA measurements showed two distinct steps of mass loss, occurring at around 100 °C (11.5 %) and around 150 °C (3.5 %), which is identified as loss of water. After ca. 250 °C decomposition is observed, which is accompanied by a loss of water, probably due to the condensation of phosphonic acid groups.[28,37] This transition is also confirmed by the in-situ temperature variable PXRD showing peaks after 200 °C, and more intensely after keeping the TUB41 crystals at 250 °C and 300 °C for longer period of time (See Figure 2b). At 400 °C still more than 75 mass-% of the sample remain, suggesting appreciable thermal stability of the organic linker molecules while the structure has potentially changed to another less crystalline phase after likely condensation of the phosphonic acids according to PXRD above 250 °C (see Figure 2b and 4 left).

5. CO_2 and water vapor adsorption studies

Both nitrogen and argon sorption isotherms were measured at 77 K, but showed only very low adsorption (Figure S3) and a BET surface area of only ca. 4 m^2/g. The CO_2 sorption in Figure 6a showed a higher adsorption and distinct hysteresis over the whole pressure range, indicating positive attractive interaction between adsorbent and adsorbate. The hysteresis looks closest to type H4,[38] further strengthening the hypothesis of small, narrow pores with a polar internal surface. BET calculations using the CO_2 adsorption isotherm at 273 K gave a surface area of 60 m^2/g and a total pore volume of 0.019 cm^3/g still showing low porosity. By measuring adsorption at three different temperatures, an estimation of the adsorption enthalpy was possible by fitting the adsorption isotherms to a Langmuir-Freundlich expression (Figure S1) and using the Clausius-Clapeyron equation (1):[39]

$$\Delta H_{\text{ads}}(n) = -R \ln\left(\frac{p_2}{p_1}\right)\frac{T_1 T_2}{(T_2 - T_1)} \quad (1)$$

with n as the loading in units of mol · g^{-1}, R = 8.314 J · K^{-1} · mol^{-1} as the gas constant, p_1 and p_2 as two reference pressures and T_1 and T_2 as the respective reference temperatures. The enthalpy of adsorption for low loadings was thus calculated as –41 kJ/mol for an adsorbed amount of 0.01 mmol · g^{-1} CO_2.

Water vapor sorption measurements at 283, 288, and 293 K showed adsorption with a slight concave curvature in the low-pressure region and a very strong hysteresis closest to type H2 (see Figure 6b).[38] Desorption at measurement temperatures was not complete, showing strong interactions and polar surfaces, but since the same sample was used for all sorption measurements, it is shown that the activation procedure between measurements, 80 °C for 2 h under vacuum, was sufficient to empty the pores. The overall adsorption is still not very high, fitting with the already measured limited porosity, but much higher than anticipated from the nitrogen adsorption measurements only, again indicating very small pores only accessible to molecules with a smaller kinetic diameter and at higher temperatures. At relative pressures between 0.7 and 0.8, inter-particle condensation began, leading to a strong increase in the amount of adsorbed water.

The enthalpy of adsorption of water was also calculated according to the same procedure as for CO_2. For computational purposes, only the low-pressure region before condensation was used. This approach resulted in a value of –38 kJ/mol for the enthalpy of adsorption for a loading of 0.7 mmol/g (pressure of 2 · 10^{-3} bar). This high loading compared to the loading with CO_2 was

chosen due to lower accuracy within the low-pressure region for water sorption and the available measurement points (Figure S2). The heat of adsorption increases with increasing pressure, probably caused by the formation of hydrogen bonds between adsorbed water molecules. Comparison to the heat of adsorption of CO_2 is difficult and further complicated by the difference between a gas and vapor, but apparently are in a similar range and both show attractive interaction with the pore surface. Despite a potentially preferential adsorption for CO_2 molecules based on the adsorption heat data, the material exhibited a higher mass of water vapor adsorption (0.04 g/g) compared to CO_2 adsorption (0.017 g/g), which might be due to the smaller kinetic diameter of water molecules (2.65 Å) compared to CO_2 (3.3 Å) in the gaseous phase. Another reason for the higher water adsorption might be due to the condensation of water molecules between the TUB41 crystals, which usually happens at higher relative pressures.

The total number of MOFs that are more selective for CO_2 in the presence of water vapor is very limited in the literature as MOFs usually have higher affinity for water vapor due to the presence of hydrophilic moieties.[15,40] Although the amount of adsorbed CO_2 is limited in TUB41 due to its small surface area, it still has a unique place among other MOFs with its narrow and selective pores limiting competition with gases having larger kinetic diameters (e. g. nitrogen (3.64 Å) and methane (3.8 Å) in atmosphere and naphthalene moieties provide more hydrophobic nature to the pores providing a more suitable enthalpy of adsorption for CO_2 gas compared to the water vapor.

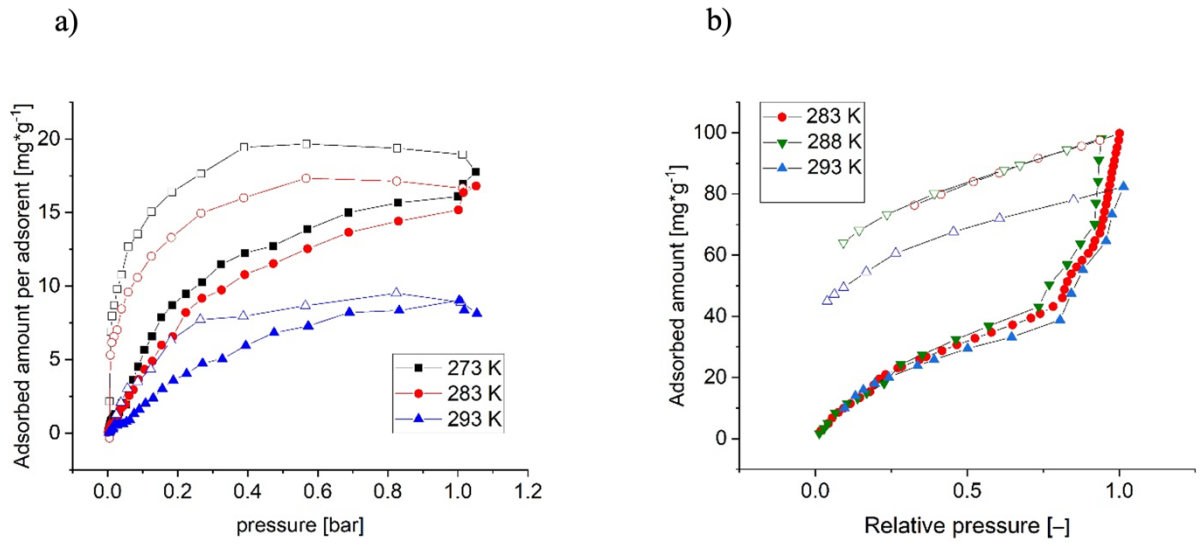

Figure 6. (a) CO_2 sorption at different temperatures (filled symbols adsorption, empty symbols desorption) (n) Water vapor sorption isotherms at 283, 293 and 303 K (filled symbols adsorption, empty symbols desorption).

All sorption measurements combined confirm the existence of very small pores, which are not accessible for both nitrogen and argon due to their higher kinetic diameter and the cryogenic measurement temperatures (see Figure S3). Ar has a slightly higher kinetic diameter of 3.4 Å compared to CO_2 which has a kinetic diameter of 3.3 Å.[41] Therefore, the upper limit for gases to enter the pores of TUB41 is between 3.3 Å and 3.4 Å. This narrow margin for CO_2 adsorption might have provided the optimum non-covalent multi-site interactions between the TUB41 pores and CO_2, which in return generated a favorable enthalpy of adsorption for CO_2 compared to water that has much smaller kinetic diameter, upon entering the TUB41 pores. Furthermore, the naphthalene moieties of TUB41 block the interaction of water molecules with the hydrophilic SBU and the mono deprotonated phosphonate groups, preventing strong hydrogen bonding interactions that could have otherwise favored the water vapor adsorption in the narrow pores of TUB41.

6. Optical properties

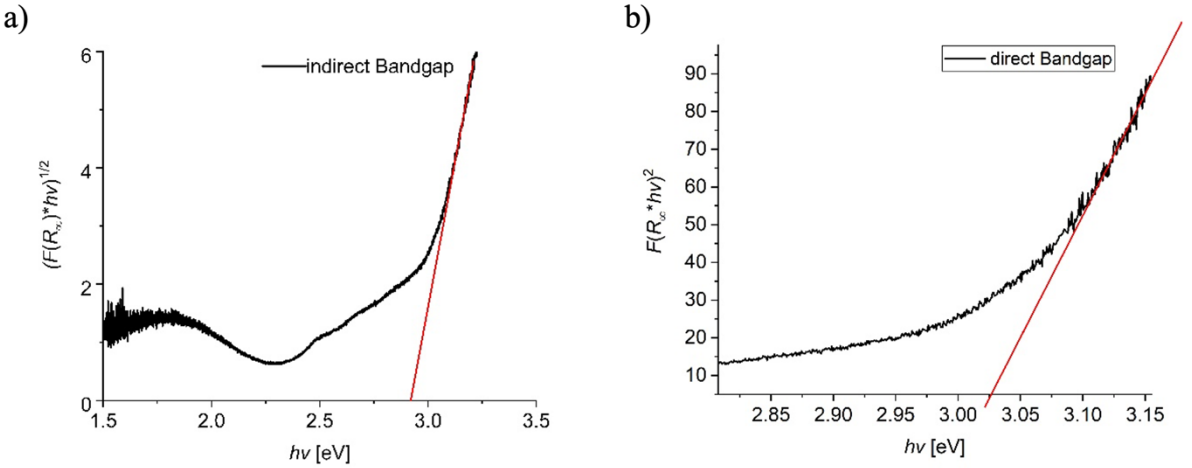

Figure 7. a) Indirect band gap and b) direct band gap of TUB41

Copper phosphonate MOFs such as TUB1, TUB40 and TUB75 are sister compounds of TUB41 and known for their semiconducting properties, which is also seen in other phosphonate MOFs.[29,42-44] Thus, we measured the diffuse reflectance spectrum of TUB41 to estimate the band gap of this compound (see Figure 7a and b). According to Tauc plots generated from the diffuse reflectance spectra, an indirect band gap of 2.7 eV or direct (optical) band gap of 3.0 eV can be estimated (see SI for experimental details).[45,46] The additionally visible band at around 1.7 eV can be related to a localized $3d^9 \leftarrow 3d^9$ transition of the Cu(II) centers ($^2E \leftarrow {}^2T_2$ in an approximately tetrahedral field). TUB41 has a very similar SBU compared to our previously

reported MOF TUB1. The SBUs in both TUB1 and TUB41 have the same order of vertex-connected [Cu–O–P–O–Cu–O–P–O] eight-membered rings resulting in a rod shaped SBU (See Figure 1b).[44] The major difference between the SBUs of TUB41 and TUB1 is the first copper atom (Cu1) in TUB1, which is coordinated in a square-planar fashion, while the second copper atom (Cu2) is coordinated in a square-pyramidal fashion. In TUB41 all copper atoms show a square-pyramidal coordination sphere. Similar to TUB41, our previously published MOF TUB1 provided an indirect band gap of 2.4 eV and a direct band gap of 2.7 eV in a similar range, which was also confirmed by DOS calculations.[44] The slightly narrower band gap observed in TUB1 might be due to the presence of square planar coordinated Cu(II) ions as indicated by the calculations in the previous work. These resulting indirect and direct band gaps in TUB41 are within the visible range indicating the potential use of TUB41 in photocatalysis.

Conclusions

TUB41 stands out among other MOFs due to its unique stability, combination of narrow, selective hydrophobic pores that limit competition with gases having larger kinetic diameter than 3.3 Å. We were able to observe the stability of TUB41 over a two years period. TUB41 provides stability at pH 2.5 for more than one month. It is also stable between pH 1 and pH 11 for at least two hours, and the crystals of TUB41 remained stable after repeated adsorption experiments and activation at 80 °C under vacuum. One of the difficulties to capture CO_2 is the presence of water vapor, which intrinsically has a higher affinity for MOFs as they are composed of hydrophilic metal binding functional groups. The naphthalene moieties incorporated into the framework of TUB41 provide enhanced hydrophobicity to the pores, resulting in a more favorable enthalpy of adsorption for CO_2 compared to water vapor. Additionally, TUB41 demonstrates exceptional chemical stability compared to the conventional MOFs (which are often hydrolyzed in the presence of water vapor), particularly in the presence of acids and bases between the pH range of 1 and 11, further enhancing its potential for industrial applications, especially as membranes that can sieve CO_2 molecules. Furthermore, the rod shaped SBU provides reversible phase transitions to TUB41 observed at different temperatures. In situ temperature variable PXRD combined with MS-TGA suggested the condensation of phosphonate groups to release additional water molecules at higher temperatures. From diffuse reflectance spectra, a band gap between 2.7 and 3.0 eV, within the bluish-violet spectral range, is estimated. The selectivity of TUB41 for water vapor and CO_2

gases and its band gap within the visible range makes TUB41 a suitable candidate for applications such as photocatalytic water splitting and electrocatalytic reduction of CO_2.

Furthermore, conventional MOFs with metal carboxylate SBUs have relatively short shelf lives. For example, UiO-66 have a shelf life of 2 months at room temperature and ambient humidity. The remarkable thermal and chemical stability of TUB41 after two years of repeated use is a significant development for industrial applications of MOFs. To the best of our knowledge, TUB41 exhibits the longest stability among other MOFs, maintaining its structural integrity for over two years and continuing to remain stable. The development of phosphonate-MOFs like TUB41 composed of non-soluble SBUs and stability in concentrated acids and bases will be key in developing next generation MOFs with the desired stability to perform applications requiring the presence of aqueous solutions, acids, bases and aqueous electrolytes.

Supporting Information

Supporting Information for the details of synthesis, gas and water sorption and optical. spectroscopy is available.

Acknowledgements

G. Y. would like to thank DFG for fundings DFG YU 267/2-1 and DFG YU 267/9-1. M. S. acknowledges funding from a materials cost allowance of the Fonds der Chemischen Industrie e.V. and a scholarship of the "Young College" of the North-Rhine Westphalian Academy of Sciences, Humanities, and the Arts. We would like to thank Microtrac Retsch GmbH to perform the N_2 and Ar adsorption work.

Author Contributions

R.O. performed the gas sorption studies and optical measurements and wrote the corresponding section. M.F. resynthesized TUB41, developed a new method for the linker synthesis, and performed the stability experiments and took SEM pictures. A.S. performed the N_2 and Ar adsorption measurements, A.K. performed the in-situ temperature variable PXRD measurements and wrote the corresponding section, M.S. supervised the optical measurements, wrote the corresponding section, and edited the manuscript. C. J. supervised the gas adsorption work, created the crystallographic figures, and edited the manuscript. G.Y. created the hypothesis, supervised the work of M.F. and R.O. and wrote the manuscript.

References

1 Furukawa, H., Cordova, K. E., O'Keeffe, M. & Yaghi, O. M. The Chemistry and Applications of Metal-Organic Frameworks. *Science* **341**, 1230444 (2013).

2 Yaghi, O. M., Kalmutzki, M. J. & Diercks, C. S. *Introduction to Reticular Chemistry: Metal-Organic Frameworks and Covalent Organic Frameworks*. (2019).

3 Beglau, T. H. Y. *et al.* Exceptionally Stable And Super-Efficient Electrocatalysts Derived From Semiconducting Metal Phosphonate Frameworks. *Chemistry – A European Journal* **30**, e202302765 (2024). https://doi.org/https://doi.org/10.1002/chem.202302765

4 Tholen, P. *et al.* A New Family of Layered Metal-Organic Semiconductors: Cu/V-Organophosphonates. *Small*, 2304057 (2023). https://doi.org/https://doi.org/10.1002/smll.202304057

5 Horcajada, P. *et al.* Metal-Organic Frameworks in Biomedicine. *Chem. Rev.* **112**, 1232 (2012).

6 Rojas, S., Arenas-Vivo, A. & Horcajada, P. Metal-organic frameworks: A novel platform for combined advanced therapies. *Coordination Chemistry Reviews* **388**, 202-226 (2019). https://doi.org/https://doi.org/10.1016/j.ccr.2019.02.032

7 Ambrogio, M. W., Thomas, C. R., Zhao, Y. L., Zink, J. I. & Stoddart, J. F. *Acc. Chem. Res.* (2011).

8 Hartlieb, K. J. *et al.* Encapsulation of Ibuprofen in CD-MOF and Related Bioavailability Studies. *Mol. Pharmaceutics* **14**, 1831 (2017).

9 Smaldone, R. A. *et al.* Metal-Organic Frameworks from Edible Natural Products. *Angew. Chem., Int. Ed.* **49**, 8630 (2010).

10 Howarth, A. J. *et al.* Chemical, Thermal and Mechanical Stabilities of Metal-Organic Frameworks. *Nat. Rev. Mater.* **1**, 15018 (2016).

11 Ding, M., Cai, X. & Jiang, H.-L. Improving MOF stability: approaches and applications. *Chemical Science* **10**, 10209-10230 (2019). https://doi.org/10.1039/C9SC03916C

12 Healy, C. *et al.* The thermal stability of metal-organic frameworks. *Coordination Chemistry Reviews* **419**, 213388 (2020). https://doi.org/https://doi.org/10.1016/j.ccr.2020.213388

13 Ding, M., Cai, X. & Jiang, H. L. Improving MOF Stability: Approaches and Applications. *Chem. Sci.* **10**, 10209 (2019).

14 Bůžek, D., Adamec, S., Lang, K. & Demel, J. Metal-Organic Frameworks vs. Buffers: Case Study of UiO-66 Stability. *Inorg. Chem. Front.* **8**, 720 (2021).

15 Lin, J.-B. *et al.* A scalable metal-organic framework as a durable physisorbent for carbon dioxide capture. *Science* **374**, 1464-1469 (2021). https://doi.org/10.1126/science.abi7281

16 Gagnon, K. J., Perry, H. P. & Clearfield, A. Conventional and unconventional metal-organic frameworks based on phosphonate ligands: MOFs and UMOFs. *Chem Rev* **112**, 1034-1054 (2012). https://doi.org/10.1021/cr2002257

17 Sevrain, C. M., Berchel, M., Couthon, H. & Jaffrès, P.-A. Phosphonic acid: preparation and applications. *Beilstein Journal of Organic Chemistry* **13**, 2186-2213 (2017). https://doi.org/10.3762/bjoc.13.219

18 Motekaitis, R. J., Murase, I. & Martell, A. E. Equilibriums of ethylenediamine-N,N,N',N'-tetrakis(methylenephosphonic) acid with copper(II), nickel(II), cobalt(II), zinc(II), magnesium(II), calcium(II), and iron(III) ions in aqueous solution. *Inorganic Chemistry* **15**, 2303-2306 (1976). https://doi.org/10.1021/ic50163a066

19 Demadis, K. D. & Stavgianoudaki, N. *Metal Phosphonate Chemistry: From Synthesis to Applications*. (2012).
20 Yücesan, G., Zorlu, Y., Stricker, M. & Beckmann, J. Metal-organic solids derived from arylphosphonic acids. *Coordination Chemistry Reviews* **369**, 105-122 (2018). https://doi.org/https://doi.org/10.1016/j.ccr.2018.05.002
21 Mah, R. K., Lui, M. W. & Shimizu, G. K. H. Enhancing Order and Porosity in a Highly Robust Tin(IV) Triphosphonate Framework. *Inorganic Chemistry* **52**, 7311-7313 (2013). https://doi.org/10.1021/ic400274e
22 Bao, S.-S., Shimizu, G. K. H. & Zheng, L.-M. Proton conductive metal phosphonate frameworks. *Coordination Chemistry Reviews* **378**, 577-594 (2019). https://doi.org/https://doi.org/10.1016/j.ccr.2017.11.029
23 Bao, S. S., Shimizu, G. K. H. & Zheng, L. M. Proton Conductive Metal Phosphonate Frameworks. *Coord. Chem. Rev.* **378**, 577 (2019).
24 Salcedo-Abraira, P. *et al.* Nickel phosphonate MOF as efficient water splitting photocatalyst. *Nano Research* **14**, 450-457 (2021). https://doi.org/10.1007/s12274-020-3056-6
25 Peeples, C. A. *et al.* A 3D Cu-Naphthalene-Phosphonate Metal–Organic Framework with Ultra-High Electrical Conductivity. *Advanced Functional Materials* **n/a**, 2007294 https://doi.org/https://doi.org/10.1002/adfm.202007294
26 Tholen, P. *et al.* Semiconductive microporous hydrogen-bonded organophosphonic acid frameworks. *Nat. Commun.* **11**, 3180 (2020).
27 Tholen, P. *et al.* Tuning Structural and Optical Properties of Porphyrin-based Hydrogen-Bonded Organic Frameworks by Metal Insertion. *Small* **18**, 2204578 (2022). https://doi.org/https://doi.org/10.1002/smll.202204578
28 Xu, K. *et al.* Polyphosphonate covalent organic frameworks. *Nature Communications* **15**, 7862 (2024). https://doi.org/10.1038/s41467-024-51950-1
29 Ribeiro, C. *et al.* Mixed Ionic and Electronic Conductivity in a Tetrathiafulvalene-Phosphonate Metal–Organic Framework. *Journal of the American Chemical Society* **147**, 63-68 (2025). https://doi.org/10.1021/jacs.4c13792
30 Siemensmeyer, K. *et al.* Phosphonate Metal–Organic Frameworks: A Novel Family of Semiconductors. *Adv. Mater.* **32**, 2000474 (2020).
31 Peeples, C. A. *et al.* A 3D Cu-Naphthalene-Phosphonate Metal–Organic Framework with Ultra-High Electrical Conductivity. *Advanced Functional Materials* **31**, 2007294 (2021). https://doi.org/https://doi.org/10.1002/adfm.202007294
32 Bulut, A. *et al.* Short Naphthalene Organophosphonate Linkers to Microporous Frameworks. *ChemistrySelect* **2**, 7050-7053 (2017). https://doi.org/https://doi.org/10.1002/slct.201701411
33 Mukherjee, S. *et al.* Trace CO2 capture by an ultramicroporous physisorbent with low water affinity. *Science Advances* **5**, eaax9171 https://doi.org/10.1126/sciadv.aax9171
34 Xue, D.-X. *et al.* Tunable Rare Earth fcu-MOF Platform: Access to Adsorption Kinetics Driven Gas/Vapor Separations via Pore Size Contraction. *Journal of the American Chemical Society* **137**, 5034-5040 (2015). https://doi.org/10.1021/ja5131403
35 Smirnova, O. *et al.* Precise control over gas-transporting channels in zeolitic imidazolate framework glasses. *Nature Materials* **23**, 262-270 (2024). https://doi.org/10.1038/s41563-023-01738-3
36 Tholen, P., Zorlu, Y., Beckmann, J. & Yücesan, G. Probing Isoreticular Expansions in Phosphonate MOFs and their Applications. *European Journal of Inorganic Chemistry* **2020**, 1542-1554 (2020). https://doi.org/https://doi.org/10.1002/ejic.201901291

37 Guo, L.-R., Bao, S.-S., Li, Y.-Z. & Zheng, L.-M. Ag(i)-mediated formation of pyrophosphonate coupled with C–C bond cleavage of acetonitrile. *Chemical Communications*, 2893-2895 (2009). https://doi.org/10.1039/B902162K

38 Sing, K. S. W. Reporting physisorption data for gas/solid systems with special reference to the determination of surface area and porosity (Recommendations 1984). **57**, 603-619 (1985). https://doi.org/doi:10.1351/pac198557040603

39 Nuhnen, A. & Janiak, C. A practical guide to calculate the isosteric heat/enthalpy of adsorption via adsorption isotherms in metal–organic frameworks, MOFs. *Dalton Transactions* **49**, 10295-10307 (2020). https://doi.org/10.1039/D0DT01784A

40 Boyd, P. G. *et al.* Data-driven design of metal–organic frameworks for wet flue gas CO2 capture. *Nature* **576**, 253-256 (2019). https://doi.org/10.1038/s41586-019-1798-7

41 Matteucci, S., Yampolskii, Y., Freeman, B. D. & Pinnau, I. in *Materials Science of Membranes for Gas and Vapor Separation* 1-47 (2006).

42 Siemensmeyer, K. *et al.* Phosphonate Metal-Organic Frameworks: A Novel Family of Semiconductors. *Adv. Mater.* **32**, 2000474 (2020).

43 Peeples, C. A. *et al.* A 3D Cu-Naphthalene-Phosphonate Metal–Organic Framework with Ultra-High Electrical Conductivity. *Adv. Funct. Mater.* **31**, 2007294 (2021).

44 Peeples, C. A. *et al.* Coordination-Induced Band Gap Reduction in a Metal–Organic Framework. *Chemistry – A European Journal* **28**, e202104041 (2022). https://doi.org/https://doi.org/10.1002/chem.202104041

45 Tauc, J. Optical Properties and Electronic Structure of Amorphous Ge and Si. *Mater. Res. Bull.* **3**, 37 (1968).

46 Tauc, J., Grigorovici, R. & Vancu, A. Optical Properties and Electronic Structure of Amorphous Germanium. *physica status solidi (b)* **15**, 627-637 (1966). https://doi.org/https://doi.org/10.1002/pssb.19660150224